Numerical Modelling the Thermal Effect on the Wildfire-Burnt Quasi-Brittle Rocks

Yifei Ma, Ph.D., P.E., M.ASCE¹ and Fahd Mohammed Naimatullah Mujahid²

¹Assistant Professor, Dept. of Civil and Architectural Engineering, Lawrence Technological University, Southfield, MI 48075. E-mail: yma@ltu.edu

²Graduate Student, Dept. of Civil and Architectural Engineering, Lawrence Technological University, Southfield, MI 48075

ABSTRACT

Increment of wildfire causes numerous disturbances and irregularities that jeopardize a sustainable society and reliable infrastructures. Due to the rigorous burns, the soil particles may breakdown due to thermal effects leading to a significant loss of the physical and mechanical properties of the soil mass, including reduced modules and strength and subsequent major problems such as soil erosion and near-surface slope slides. Many ambiguities are tied up with the multi-physics process of wildfire-burnt soil, the vegetation anchoring effect on soil strength, and the alteration of microscale soil properties. This study presents an innovative thermal-mechanical coupled model to simulate rock damage and breakage during heating-cooling processes. A series of simulations are carried out to capture the behaviors of rock samples under heating-cooling and subsequent compressive loadings using a two-dimensional discrete element method (DEM) model. The results suggest that the effect of mild wildfire on the strength and modulus reduction of rock is negligible. But the reduction of strength and modulus could be as high as 53% and 12%, respectively, under severe wildfire conditions.

Keywords: wildfire; damage evolution; thermal effect; discrete element method

INTRODUCTION

Wildfires have become an increasingly common natural disaster in many parts of the world, causing significant damage to forests, wildlife, human infrastructures (e.g., power grid (Arab et al. 2021; Vazquez et al. 2022)), and the environment. While the immediate effects of wildfires are often devastating, the long-term impacts can be equally severe or even more disastrous (Abdollahi et al. 2023; Lucas-Borja et al. 2022). When a wildfire burns through vegetation and soil, it heats the ground and causes significant changes in soil physical and mechanical properties (Agbeshie et al. 2022; Martínez et al. 2022; Memoli et al. 2022). The subsequent slow or rapid cooling process also plays a crucial role in the damage evolution and accumulation (Ebel 2012; Mol and Grenfell

2022). The heating-cooling environmental conditions can significantly alter soil moisture content, micro-fabric of the grains, and shear strength, which can have a profound impact on the stability of the hillslope potentially leading to increased risks of catastrophic slides (Keeley et al. 2009; Vajda et al. 2020).

These thermal effects usually occur at the particle scale, which is difficult to assess or quantify from *in-situ* or laboratory tests due to the spatial and temporal limitations (Beatty and Smith 2013; Peduto et al. 2022; Wieting et al. 2017). To gain a better understanding of the short-and long-term effects of wildfire on hillslope stability, researchers have turned to advanced numerical methods. Both continuum- and discontinuum-based models have been developed to capture the complex interactions between fire, soil, and vegetation to provide insights into the short- and long-term impacts of wildfires on the landscape. These models can help researchers and policymakers better understand the processes that affect hillslope stability after a wildfire and develop effective strategies to mitigate these effects. Martin (2007) applied a stochastic rule set to model the shallow land sliding induced by a wildfire and successfully captured the wildfire and sediment transport pattern resulted from the landslide. To refine the simulation results, McGuire et al. (2019) applied the vegetation and hydrologic measurements and adopted a high-resolution DEM to study the debris flow behaviors in a post-wildfire condition. The debris flow can also be simulated with a finite element model (FEM) to capture the interactions with a flexible rockfall mitigation structures (Debelak et al. 2021).

All the successful numerical models were mostly focusing on the slope-scale soil behaviors or slope-wildfire interactions, the alteration of the geo-material properties during or shortly after a wildfire was rarely considered. To bridge the gap, an innovative softening contact model coupled with a thermal pipe model is developed in this study focusing on the micro-scale behaviors. Outcomes of the numerical study will help identify the governing factors leading to the rock strength degradation and catastrophic slope slides in a wildfire environment; thus, inspire new methods and techniques to remediate the hillslope and therefore improve the stability of the near-surface rock mass. The numerical study presented in this work also promotes a fundamental understanding of the behavioral evolutions of rock mass. Particularly, the outcomes reveal the thermal effect on rock mass properties under extreme wildfire environments.

MODEL SETUP

A thermal-mechanical coupled model is developed in this study to capture the heating-cooling induced micro-damages and macro-scale fracture evolution. This model is then implemented in PFC2D 7.0 (Particle Flow Code in two dimensions) (Itasca Consulting Group 2021), a software based on the discrete element method. The modeling parameters are calibrated to match a typical sandstone; however, no attempt was made to match the properties of the synthetic rock to a specific rock specimen.

To capture the properties of a typical sandstone, a numerical sample with a domain size of width W = 15 mm and height H = 30 mm was filled with spherical particles ranging from 0.25

to 0.5 mm, which is representative of common sandstone particle sizes (Ahad et al. 2020). The baseline sample, as shown in Figure 1, consists of 3,539 particles. The interactions of the particles are governed by the mechanical forces calculated from a displacement-softening contact law combined with thermal forces induced by the thermal expansions and contractions. Considering the relatively small sample size, gravitational force is insignificant and can be neglected.

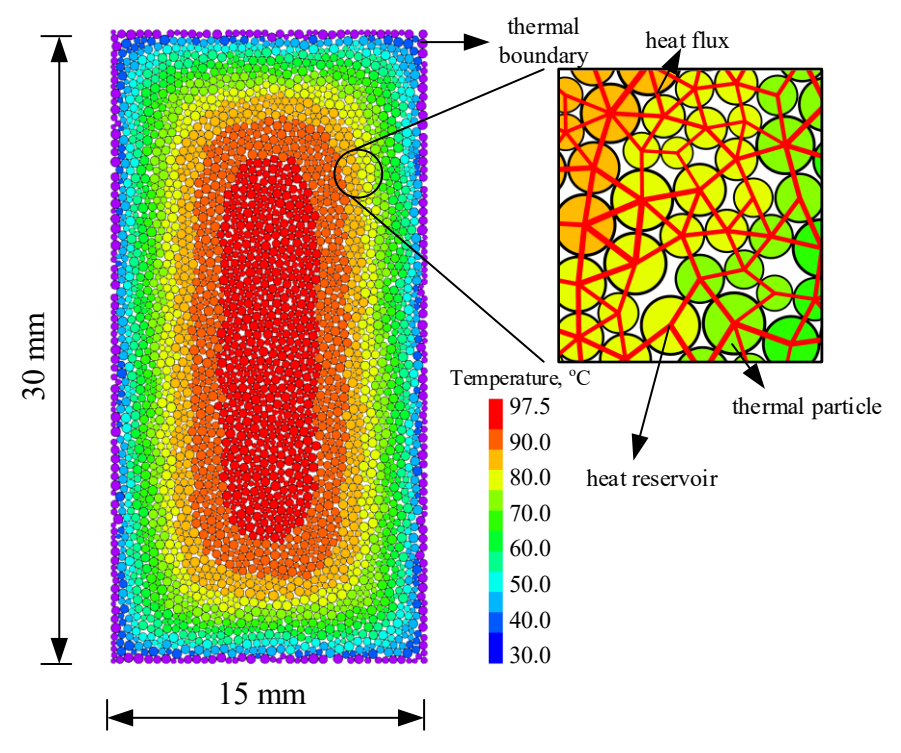


Figure 1. Thermal-mechanical coupled model.

The sample is heated or cooled from the exterior by specifying a thermal boundary condition. The exterior particles are assigned to a constant temperature until an allowable temperature gradient is achieved throughout the whole sample. Then a small temperature increment is added or deducted to the thermal boundary particles to simulate the heating or cooling process, respectively. To guarantee a stable condition (i.e., no sudden outstanding temperature gradient changes during the simulation), the heating and cooling is performed in a ramp-up or ramp-down fashion corresponding to the heating and cooling process, respectively. The thermal boundary particles will be eventually assigned the target temperature and maintained a constant until the sample reaches a thermal equilibrium state, where the center temperature of the sample is within 1% difference compared to the temperature of the thermal boundary particles. Then the heated or cooled sample will be used for subsequent compression tests. In this study, the sample is first heated from ambient temperature of 20 °C to a target temperature ranging from 100 °C to 1,200 °C corresponding to mild to severe wildfire conditions near the surface, then cooled to the ambient temperature again. After the heating-cooling cycle, the rock sample will be subjected to the unconfined compression test. All tests are performed in a quasi-static condition where the loading strain rate is at least three orders of magnitude lower than the p-wave velocity within the

sample. A micro-damage and crack tracking mechanism is installed during the simulations to study the evolution of thermal-induced cracks. The inter-particle forces are realized through the mechanical contact model and the thermal pipe model.

Mechanical Model

In this study, a displacement-softening contact model (Ma and Huang 2018) modified from the parallel bond option in PFC is used to simulate the initiation, accumulation, and evolution of micro-damages.

Figure 2 shows the force-displacement law at the contact bond between two contacting particles, when the equivalent distance between the particles is within δ_1 , all the input energy is converted into elastic energy, i.e., no energy is dissipated during the loading process. But when the distance exceeds δ_1 , a certain amount of elastic energy is released due to plasticity (i.e., microdamages). Then the contact force will be reduced following the softening curve with a slope of $\beta \bar{k}_l$, where β is the softening coefficient and \bar{k}_l is the loading stiffness when bonding is intact. Previous studies have shown that the softening coefficient $\beta = 0.1$ will yield the compressive to tensile strength ratio to be approximately equal to 10, which is within the typical range of common sandstones (Ma and Huang 2017, 2018). The softening behavior is only installed in the normal direction at the contact point considering the fact that the damages in tangential directions has minimum impact on the macro-scale failure patterns (Ma and Huang 2021).

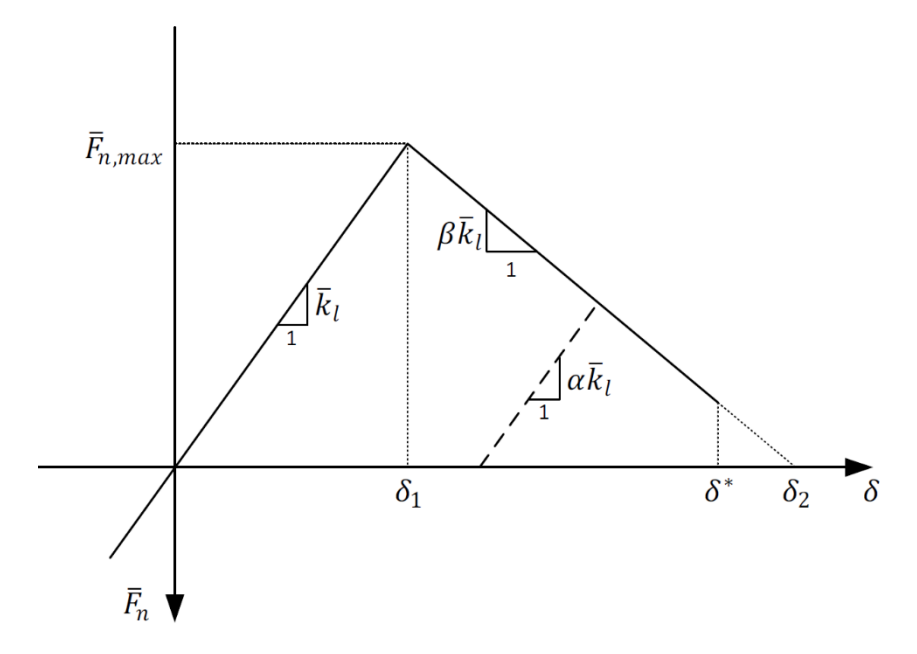


Figure 2. Force-displacement law of the contact model (Source: Ma and Huang 2018).

Damage initiates when the normal contact force \bar{F}_n in the bond reaches a limit defined by the parallel bond strength $\bar{\sigma}_c$, i.e.,

$$\bar{F}_{n,max} = \bar{\sigma}_c \cdot \bar{A} \tag{1}$$

where \bar{A} is the cross-sectional area of the bond and $\bar{A}=2\bar{R}$ in 2D assuming unit thickness in the out-of-plane direction; \bar{R} is the minimum radius of the two contacting bodies. The force-displacement relationship during the softening stage is expressed as,

$$\delta_n = \frac{\overline{\sigma}_c}{\overline{k}_n} + \frac{\overline{\sigma}_c - \overline{F}_n / \overline{A}}{\beta \overline{k}_n} \tag{2}$$

where \bar{k}_n is the normal stiffness for the parallel bond.

The bond fails if one of the following two criteria is satisfied:

$$\delta_n + \bar{R}|\theta| > \delta_c$$
 or $\bar{F}_s/\bar{A} > \bar{\tau}_c$ (3)

where θ is the relative angle of rotation between the two particles and δ_c is the critical displacement of the parallel bond. In this study the cohesion $\bar{\tau}_c$ (i.e., shear strength of the bond) is set to be two orders of magnitude higher than the normal bond strength; therefore, all microdamages will be governed by the first failure criterion. If the maximum stretch of the bond reaches the threshold value of δ_c , the bond will break. The critical stretch δ_c is expressed as,

$$\delta_c = \frac{\overline{\sigma}_c}{\overline{k}_n} \left(\frac{1+\beta}{\beta} \right) \tag{4}$$

After bond breaks, only frictional forces remain. Such behaviors are characterized using the normal and shear stiffnesses at the contact point, k_n and k_s , and the friction coefficient μ .

Thermal Model

The thermal pipe contact model is implemented to simulate the heat exchange between contact particles. Each particle is considered a temperature-independent heat reservoir and the heat exchange can only occur through thermal contacts envisioned as thermal pipes when the temperature difference is non-zero, see Figure 1. The heat flux q can be calculated via Fourier's law as,

$$q = -k \frac{\partial T}{\partial x} \tag{5}$$

where k is the thermal conductivity, and $\partial y/\partial x$ is the temperature gradient between the two heat reservoirs. The thermal expansion (or contraction) of particles, ΔR , caused by temperature change, ΔT , can be calculated as,

$$\Delta R = \alpha \cdot R \cdot \Delta T \tag{6}$$

where R is the particle radius and α is the thermal expansion coefficient. Assuming the sample is thermally isotropic, the thermally induced force caused by the thermal expansion (or contraction) can be calculated as,

$$\Delta \bar{F}_n = -\bar{k}_n \bar{A} (\alpha \bar{L} \cdot \Delta T) \tag{7}$$

where \bar{L} is the center-to-center distance between the two contacting particles, i.e., the length of the thermal pipe. A thermal material is discretized into a network of thermal reservoirs connected with thermal pipes. The calculation of the thermal conductivity tensor requires the calculation of the control volume, which can be problematic in DEM models. Therefore, the calculation is simplified by assuming a thermally isotropic material, where the thermal conductivity tensor becomes a single parameter k, related to the thermal resistance η by the following equation:

$$\eta = \frac{1}{2k} \left(\frac{1-n}{\sum_{N_h} V_b} \right) \sum_{N_p} L_p \qquad \text{in 2D}$$
 (8)

where n is local porosity; N_b is number of particles in the representative elementary volume (REV); V_b is the total volume of solid particles; N_p is the total number of thermal pipes within the REV; and L^P is the length of thermal pipes associated with particles in the REV.

When temperature change occurs, the particle size will expand or contract accordingly, proportional to the thermal expansion coefficient. The specific heat C_v of the material controls how much energy is needed for the temperature to change by one degree per unit mass. Considering this parameter only controls how fast the temperature change occurs and has minimum impact on the final results, C_v is scaled down by a factor of 10^{-3} for a higher simulation efficiency.

Model Calibration and Validation

The micro-scale parameters for the thermal-mechanical coupled model are summarized in Table 1. The parameters are calibrated to match a typical sandstone with macro-properties summarized in Table 2. The micro-parameters can be easily adjusted to match a specific rock sample if needed. However, no attempt was made in this study to fine-tune the parameters to match experimental results from a specific specimen.

The calibrated parameters remain constant for all the series of the simulations in this study. The baseline sample, labeled as BL, is first tested under the uniaxial compression and direct tension tests to justify the macro-scale properties and compare with typical values of sandstone. The stress-strain curve is recorded and analyzed. The stress is calculated using the wall force measurements. The axial strain is determined based on the displacement of the moving walls. After the baseline simulations, the digital sample is heated to a target temperature T_{tar} following a ramp-up fashion as introduced previously. Then the sample is cooled back to the ambient temperature. During the whole heating-cooling process, the walls confining the sample are moved away to avoid boundary effects. However, by the end of the heating-cooling process, the loading walls (i.e., horizontal top and bottom walls) are moved back to the original location. Due to the sample disturbance caused by the thermal effects, the initial contact forces at the walls are no longer zero. Therefore, the reference gap at the wall-particle contact is manually reset to be equal to the current gap. Thus, the

compression test always starts with a consistent initial condition where the contact force at the loading walls is zero.

Table 1: Micro parameters

Parameter	Value	Remark
General Parameters		
Particle size (mm)	0.25 - 0.5	Uniform distribution.
Sample height (mm)	30	Aspect ratio of the sample is 2:1.
Sample width (mm)	15	
Porosity (%)	10	Isotropic dense packing.
Grain density (kg/m³)	2450	Typical sand.
Mechanical Model Parameters		
Friction coefficient	0.4	
Friction angle (deg)	35	Typical value for sand.
Local damping	0.7	Reduce simulation time to reach equilibrium.
Normal to shear stiffness ratio	1.5	
Effective modulus (GPa)	3	Calibrated to match a typical sandstone.
Softening coefficient	0.1	Maintain a realistic strength ratio of 10.
Tensile bonding strength (MPa)	5	Calibrated to match compressive strength.
Cohesion (MPa)	500	100 times higher than tensile bond strength.
Thermal Model Parameters		
Specific heat $(J/(kg \cdot K))$	0.79	Scaled by a factor of 10 ⁻³ for efficiency.
Thermal conductivity (W/mK)	3.36	Typical value for sandstone.

Table 2: Macro properties of the baseline model

Parameter	Value	Typical Range for Sandstone
Compressive strength (MPa)	33	2 - 32
Tensile strength (MPa)	3.3	0.2 - 4
Elastic Modulus	25.65	11.3 - 40

RESULTS

Stress-Strain Curve

In this study, the severity of wildfires is categorized into three groups, as shown in Table 3. The target heating temperature T_{tar} ranges from 200 °C to 1200 °C, which covers the surface temperature corresponding to mild to severe wildfire conditions.

Table 3: Severity of wildfire and surface temperature

Severity	Surface Temperature (°C)
Mild	< 600
Medium	$600 \sim 1000$
Severe	> 1000

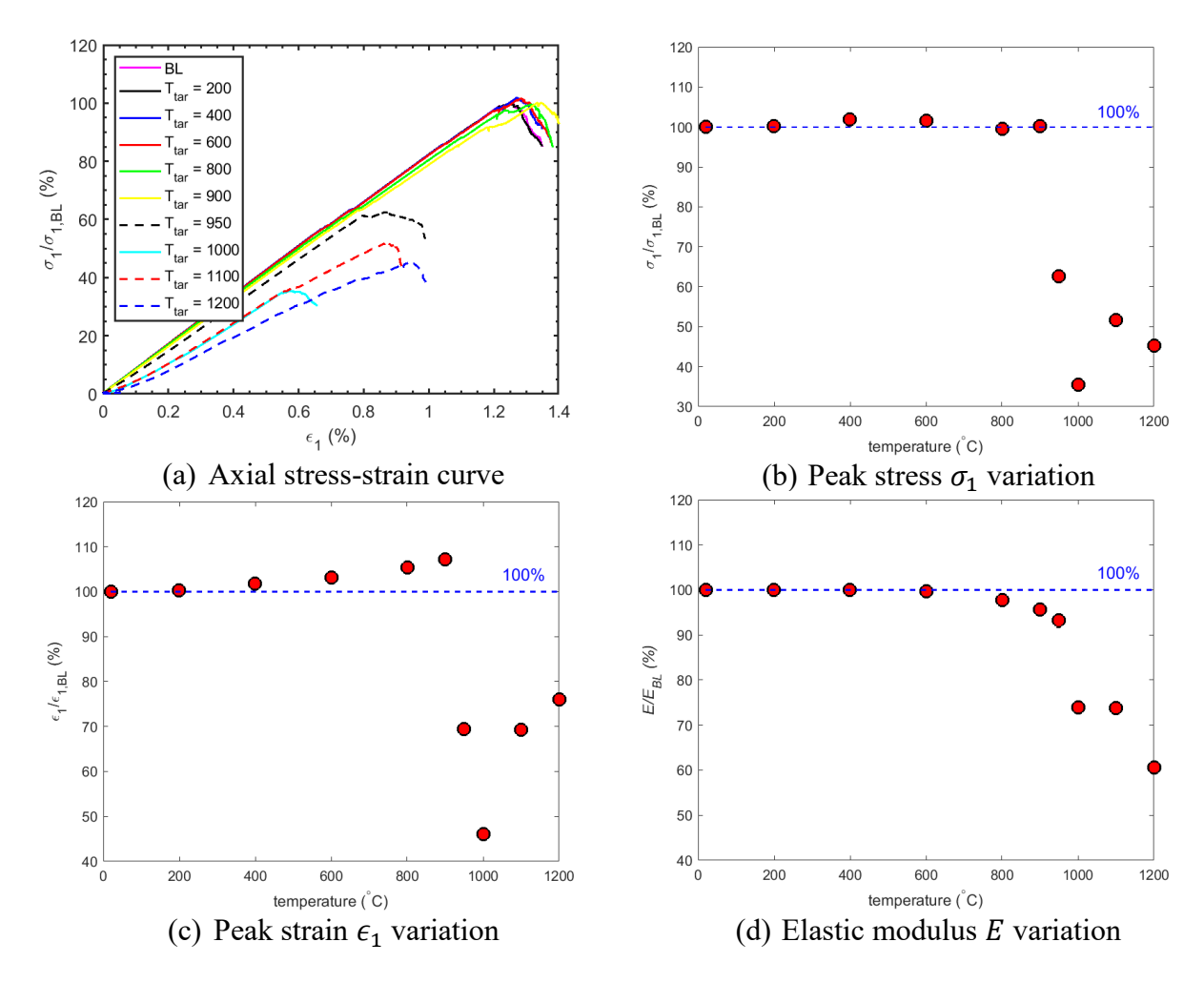
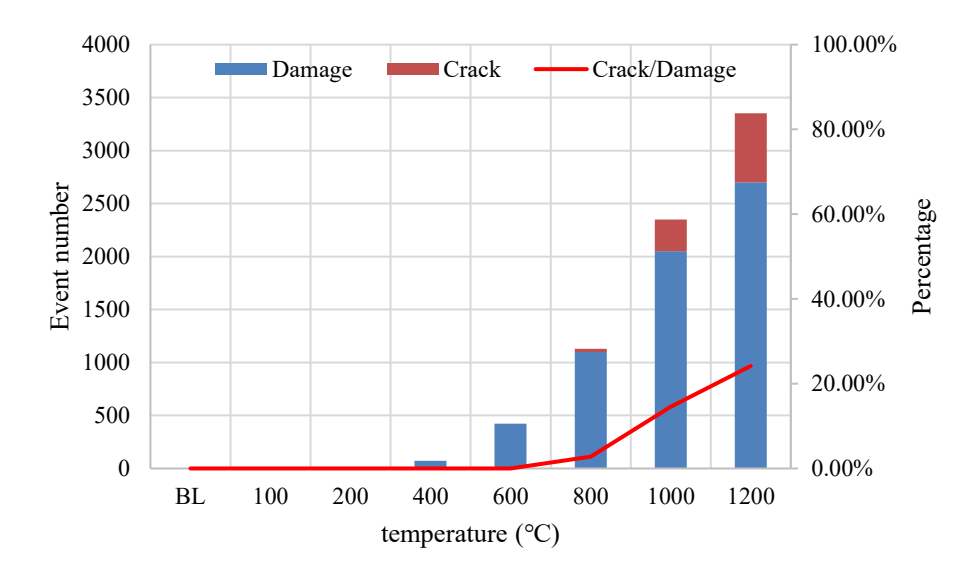


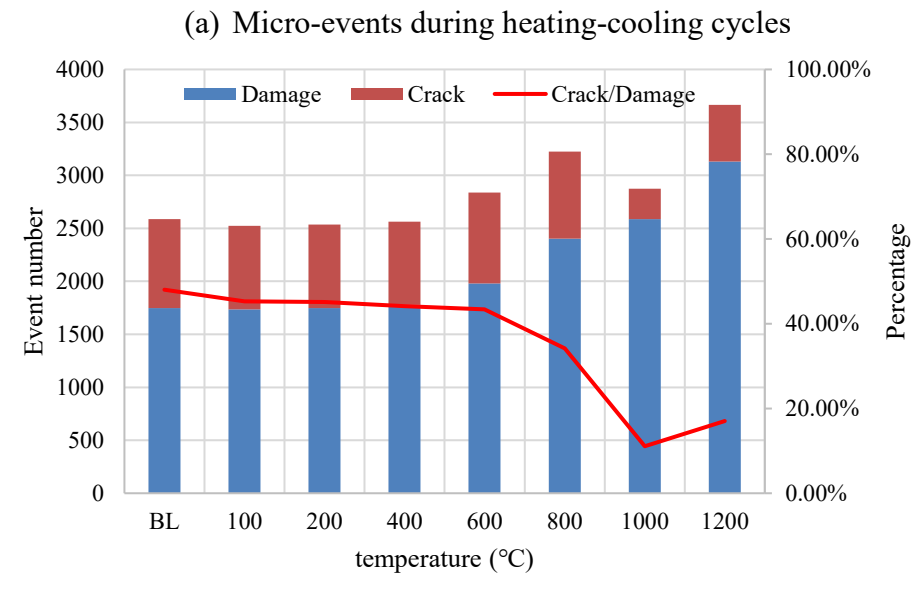
Figure 3. Mechanical property variation with the heating temperature.

The stress-strain curves from the uniaxial compression tests are summarized in Figure 3(a). The axial stress is normalized with respect to that from the baseline simulation. The peak axial stress and the corresponding strain at different heating temperatures are presented in Figure 3(b)-(c). At low heating temperatures up to 800 °C, the stress-strain curves remain roughly the same as the baseline model. However, a slight increase (i.e., less than 5%) of the peak stress and the corresponding strain is observed.

At 400 °C, the peak compressive strength is increased by 2% compared to the baseline. Statistically, the increment is negligible; however, a consistent trend of ascending followed by descending of the peak strength as the heating temperature increases up to 800 °C was observed from multiple series of simulations. A careful examination of the simulation results shows that the near-surface cracks due to the low heating temperature can lead to the peal-off damage of the sample surrounding the exterior boundary. When the sample is subjected to the compressive stress, the actual height to width ratio is slightly decreased from the original configuration of H/D = 2. Also, due to the size-effect, a slightly smaller sample (i.e., core sample after peel-off damage) will

yield a relatively higher compressive strength. The sample core is nearly intact under low heating-cooling temperatures.





(b) Micro-events during compression tests

Figure 4. Statistics of micro-damages and cracks during heating-cooling and compression tests.

As the heating temperature increases to T > 1000 °C, the number of micro-cracks cumulated during the heating-cooling process becomes more significant, leading to a strength and modulus reduction by 53% and 12%, respectively.

Micro-Crack Evolution

During heating-cooling, the total number of micro-damages and cracks are increasing rapidly with the heating temperature, as shown in Figure 4(a). Particularly, the crack/damage ratio is increased

to approximately 24% at the 1200 °C. On the other hand, the total number of micro-damages and cracks during compression tests is roughly maintained at a constant level during mild wildfire, see Figure 4(b). Under medium and severe wildfire, the thermally induced damage was observed throughout the whole sample during heating-cooling, rather than just near the surface as in mild wildfire. The significant increment of the number of damages leads to the weakening of the sample and a low crack/damage ratio. For example, the crack/damage ratio is decreasing from the baseline case of 48% to 17% at 1200 °C.

CONCLUSION

In this work, the thermal-mechanical model is implemented to study the thermal effect on quasibrittle rocks in wildfire environment. The results show that the thermal effect on the engineering behaviors of a quasi-brittle rock is nearly negligible if the heating temperature is relatively low. However, as the temperature exceeds a certain threshold value, the engineering behaviors of the quasi-brittle rock is abruptly reduced that can potentially trigger a catastrophic land slide. Based on the simulations results we can draw the following conclusions:

- 1. The elastic modulus is reduced by a maximum of 40% at severe wildfire conditions. The descending trend is relatively smooth and it is governed by the peak heating temperature.
- 2. Under mild wildfire conditions, the uniaxial compressive strength is not significantly altered by the heating-cooling process due to the micro-damages are mostly located near the surface. However, when a severe temperature gradient is applied, damages can initiate from the core of the sample leading to a significant reduction of the strength.
- 3. The strain corresponding to the peak stress is continuously increasing up to about 800 °C then suddenly reduced by approximately 50%. This phenomenon is mostly related to the peel-off damage surrounding the exterior boundary. As the temperature continuous to increases, the peak strain shows a reversed trend and increased to approximately 75% of the baseline case.
- 4. Under mild to medium wildfire severity, the thermally induced micro-damages are nearly negligible. However, as the temperature gradient increases, the total number of the micro-cracks abruptly increases. The crack to damage ratio is also increasing to approximately 24%. During compression, the total number of micro-damages and cracks are nearly constant. However, the crack to damage ratio is decreasing as the heating temperature is increasing, indicating the sample becomes more ductile.

ACKNOWLEDGMENTS

The work described herein was partially funded by the National Science Foundation under grant no. 2153370. The numerical simulations are also supported by the ITASCA Education Partnership Program. These supports are gratefully acknowledged and appreciated.

REFERENCES

- Abdollahi, M., Vahedifard, F., and Tracy, F. T. (2023). "Post-Wildfire Stability of Unsaturated Hillslopes Against Rainfall-Triggered Landslides." *Earth's Future*, 11(3).
- Agbeshie, A. A., Abugre, S., Atta-Darkwa, T., and Awuah, R. (2022). "A review of the effects of forest fire on soil properties." *Journal of Forestry Research*, Springer Nature Singapore, 33(5), 1419–1441.
- Ahad, N. A., Jami, M., and Tyson, S. (2020). "A review of experimental studies on sand screen selection for unconsolidated sandstone reservoirs." *Journal of Petroleum Exploration and Production Technology*, Springer International Publishing, 10(4), 1675–1688.
- Arab, A., Khodaei, A., Eskandarpour, R., Thompson, M. P., and Wei, Y. (2021). "Three Lines of Defense for Wildfire Risk Management in Electric Power Grids: A Review." *IEEE Access*, 9, 61577–61593.
- Beatty, S. M., and Smith, J. E. (2013). "Dynamic soil water repellency and infiltration in post-wildfire soils." *Geoderma*, 192(1), 160–172.
- Debelak, A, Bareither, C., and Mahmoud, H. (2021). "Coupled Numerical Simulation of Debris Flow-Soil-Structure Interactions for Flexible Barrier Mitigation Systems (MPC-21-438)."
- Ebel, B. A. (2012). "Impacts of Wildfire and Slope Aspect on Soil Temperature in a Mountainous Environment." *Vadose Zone Journal*, 11(3).
- Itasca Consulting Group. (2021). PFC 7.0 Manual. Minneapolis, MN.
- Keeley, J. E., Safford, H., Fotheringham, C. J., Franklin, J., and Moritz, M. (2009). "The 2007 southern California wildfires: Lessons in complexity." *Journal of Forestry*, 107(6), 287–296.
- Lucas-Borja, M. E., Jing, X., Van Stan, J. T., Plaza-Álvarez, P. A., Gonzalez-Romero, J., Peña, E., Moya, D., Antonio Zema, D., and de las Heras, J. (2022). "Changes in soil functionality eight years after fire and post-fire hillslope stabilisation in Mediterranean forest ecosystems." *Geoderma*, 409(October 2021).
- Ma, Y., and Huang, H. (2017). "Tensile Strength Calibration in DEM Modeling." 51st US Rock Mechanics/Geomechanics Symposium.
- Ma, Y., and Huang, H. (2018). "A displacement-softening contact model for discrete element modeling of quasi-brittle materials." *International Journal of Rock Mechanics and Mining Sciences*, 104, 9–19.
- Ma, Y., and Huang, H. (2021). "Effect of shear bond failure on the strength ratio in DEM modeling of quasi-brittle materials." *Acta Geotechnica*, Springer Berlin Heidelberg, 16(8), 2629–2642.
- Martin, Y. E. (2007). "Wildfire disturbance and shallow landsliding in coastal British Columbia over millennial time scales: A numerical modelling study." *Catena*, 69(3), 206–219.
- Martínez, S. I., Contreras, C. P., Acevedo, S. E., and Bonilla, C. A. (2022). "Unveiling soil temperature reached during a wildfire event using ex-post chemical and hydraulic soil analysis." *Science of the Total Environment*, 822.
- McGuire, L. A., Rengers, F. K., Kean, J. W., Staley, D. M., Tang, H., and Youberg, A. M. (2019). "Looking through the window of disturbance at post-wildfire debris-flow hazards." Debris-Flow Hazards Mitigation: Mechanics, Monitoring, Modeling, and Assessment - Proceedings of the 7th International Conference on Debris-Flow Hazards Mitigation, (Id), 516–523.
- Memoli, V., Santorufo, L., Santini, G., Ruggiero, A. G., Giarra, A., Ranieri, P., Di Natale, G.,

- Ceccherini, M. T., Trifuoggi, M., Barile, R., De Marco, A., and Maisto, G. (2022). "The combined role of plant cover and fire occurrence on soil properties reveals response to wildfire in the Mediterranean basin." *European Journal of Soil Biology*, Elsevier Masson SAS, 112(June), 103430.
- Mol, L., and Grenfell, M. (2022). "Influence of landscape moisture sources and topography on rock weathering patterns associated with wildfire." (February), 1761–1777.
- Peduto, D., Iervolino, L., and Foresta, V. (2022). "Experimental Analysis of the Fire-Induced Effects on the Physical, Mechanical, and Hydraulic Properties of Sloping Pyroclastic Soils." *Geosciences (Switzerland)*, 12(5).
- Vajda, V., Mcloughlin, S., Mays, C., Frank, T. D., Fielding, R., Tevyaw, A., Lehsten, V., Bocking, M., and Nicoll, R. S. (2020). "End-Permian (252 Mya) deforestation, wildfires and flooding An ancient biotic crisis with lessons for the present." *Earth and Planetary Science Letters*, Elsevier B.V., 529, 115875.
- Vazquez, D. A. Z., Qiu, F., Fan, N., and Sharp, K. (2022). "Wildfire Mitigation Plans in Power Systems: A Literature Review." *IEEE Transactions on Power Systems*, IEEE, 37(5), 3540–3551.
- Wieting, C., Ebel, B. A., and Singha, K. (2017). "Quantifying the effects of wildfire on changes in soil properties by surface burning of soils from the Boulder Creek Critical Zone Observatory." *Journal of Hydrology: Regional Studies*, Elsevier, 13(July), 43–57.